16

Super-Resolution Object Recognition Approach for Complex Edged Objects by UWB Radar

Rahmi Salman and Ingolf Willms
Fachgebiet Nachrichtentechnische Systeme,
Universität Duisburg-Essen, 47057 Duisburg
Germany

1. Introduction

Technical investigation, research and development in the wide field of security technology have been increased in recent years. Robotics as a great deal of this progress aims at advanced mobile security robots that can measure their surrounding environment accurately and provide various sensing applications. These robots will gain a steady increasing importance in private homes, industry and military. Such robots equipped with Ultra Wideband (UWB) Radar are promising for near field, non-contacting and non-destructive sensing technologies. Compared to optical or infrared systems UWB Radar does not need a visual LOS condition which makes it suitable for smoke and dust filled emergency scenarios. In contrast to common CW-Radar, due to the wide frequency band which corresponds to a high resolution in time domain, UWB Radar is possible to separate multiple reflections of multipath propagation in sub-centimetre range. Because of the presence of low frequencies UWB Radar systems are able to penetrate dielectric materials to perform subsurface imaging. Hence, UWB has superior advantages compared to classical near-field sensing technologies which make it an ideal candidate for security robots.
The object recognition (OR) method proposed in this work is part of a super-resolution Radar imaging system by backscattered UWB signals on the basis of a reference data set. The purpose of this method is detection, recognition and classification of unknown objects.

2. System setup and system design

Radar imaging is an active remote sensing technique meaning that the scene to be imaged is illuminated by a wave transmitted by the Radar system. The receiver of the system measures the variation of the electromagnetic field intensity over time collecting echoes which contain geometrical feature information of the area in the antennas footprint. The goal of the data processing is to generate a visual image of the target from the received electro-magnetic field. To get proper and sufficient information it is necessary to scan the scene, i.e. move the sensors along a certain trajectory and record UWB pulses. In case of UWB Radar, the measured pulse approximates the channel impulse response either directly or after post-processing. Plotting the measured channel impulse responses in a 2D Radarmatrix with the time-of-flight or the distance versus the antenna position leads to a so called radargram with the amplitude indicating the intensity of the received field. The

radargram is a convenient way of illustrating results of measurements and is the preferred method of displaying Radar data for further post-processing.

2.1 Objects under test and reference alphabet

The investigated objects and the reference alphabet derived from these consist of simple canonical and some polygonal complex objects in the form of beams with no variance in the 3rd dimension. In figure 1 the used 12 objects are shown.

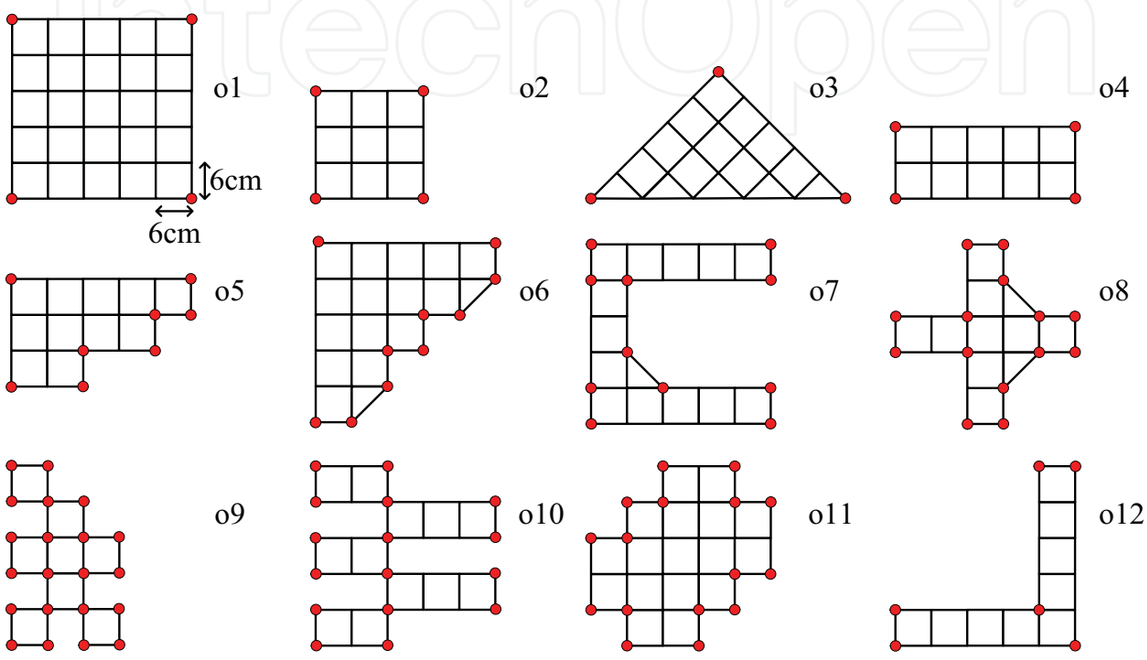

Fig. 1. Cross-section of the used 12 objects and the reference alphabet (abstracted objects consisting only discrete values equal red dots)

The reference alphabet is extracted out of a priori known dimensions of each object and consists of discrete values which are marked in figure 1 with red dots. For this purpose every edge and corner of each object is marked as a pixel with a value of 1 in a 1000 x 1000 pixel grid according to 1 mm distance between two neighboured pixels. Straight segments of the object are neither sampled nor set in any other way as a pixel at first. Hence, in the rest of the reference image pixels are set to 0 yielding to binary reference images by means of the subsequent recognition process is performed.

2.2 Simulated and measured radar data

The performance investigations of the introduced OR algorithm are carried out based on simulated Radar data obtained by Ray Tracing. To enable a quantitative proving of the effectiveness of the proposed OR algorithm, the geometric structures of each massive object were modelled by polygons and fed into the aforementioned simulation tool, which is described in its basics in (Geng & Wiesbeck, 1998; Schultze et al., 2008). The similarity between these simulations and real measurements is significantly high which could be verified in (Salman et al., 2008). In each of the 12 investigated scenarios one of the objects of

figure 1 was located in the middle of a room of 10x10 m² size and a height of 4 m. In these scenarios a quasi-monostatic antenna configuration (one antenna above the other) was moved around each object on a circular track with a radius of 1 m and at a constant level above the floor. Here, the antennas perform a scan with a 1 degree grid resulting in 360 impulse responses of a corresponding radargram. A frequency band between 2.5 and 12.5 GHz with 1601 frequency points was used. This corresponds to a frequency resolution of 6.25 MHz and thus to an unambiguous range of 48 m or 160 ns which is sufficient for most of indoor scenarios. Also antenna characteristics have been taken into account in the simulations. Here, two double-ridged horn antennas are applied. These antennas have approximately 20° opening angle (3 dB less than maximum beyond this angle). Their patterns have been measured in an anechoic chamber for all frequencies in the considered frequency band and were convoluted with the simulated channel impulse responses.
Nevertheless, experimental validations were started to complement these investigations and therefore objects o2 – o7 were built in same dimensions and scanned with same track and same antennas which were analyzed by the Ray Tracer. The used sensor system consists of a UWB Maximum Length Binary Sequence (M-Sequence) Radar system for data acquisition. Compared to pulse Radar, the energy of the transmitted waveform is spread equally over time when using an M-sequence Radar thus eliminating the power spikes of short pulses. This provides reduction of complexity and costs for the analogue electronics in the Radar device which do not need to handle high-power short-time signals thus allowing for a cheaper hardware implementation. The block diagram of an M-sequence Radar is given in figure 2.

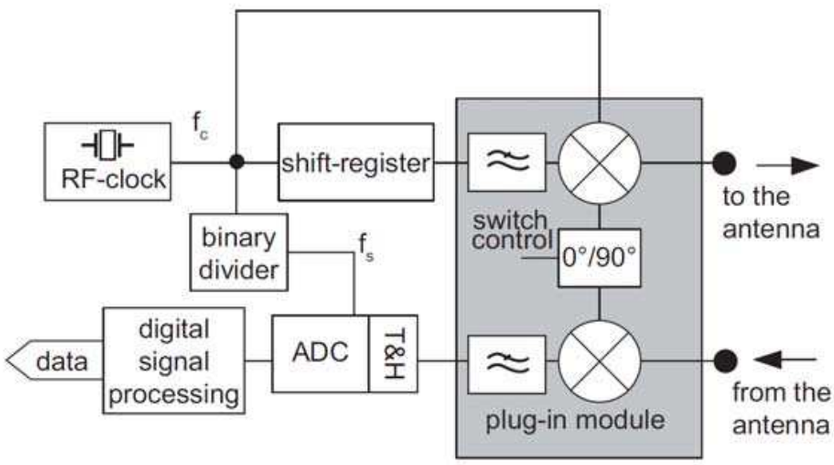

Fig. 2. Basic structure of an M-Sequence Radar with attached IQ Up/Down-converter

The shift register generates periodically (using a ring-register) the binary M-sequence with the clock frequency f_c which is the stimulus signal. The M-sequence is a special binary pseudo random code which has a very short triangular auto-correlation function. Due to Nyquist the range of the frequency spectrum is DC - $f_c/2$ meaning that the width of the pulse is adjustable directly by the clock frequency. This signal is sent to the Tx port of the device. The Tx port can either be connected directly to the transmit antenna for baseband transmission (DC - 4.5 GHz) or an additional IQ up-converter can be used which modulates

the waveform to a carrier frequency of 9 GHz for passband transmission. The reflected signal is received by the receive antenna, downconverted to baseband (if the IQ up-converter is employed) and sampled. In most wideband RF-systems, the data gathering is based on sub-sampling in order to reduce the data throughput, this is also the case with the M-sequence Radar. Usually the sampling time control is a challenging task but this is not the case for M-sequence sub-sampling, since a simple binary divider does this job in a very stable way by keeping an absolute linear (equivalent) time base of the captured signal. The divided pulse directly pushes the ADC and the track and hold circuit (T&H). The T&H captures the wideband input signal and provides it to the ADC which can work at a suitable low sampling rate f_s. In order to increase the signal to noise ratio, it is of advantage to apply synchronous averaging in the digital domain. More detailed information can be found in (Sachs et al., 2005).

2.2 Sensor track

The emulation of the free movement of a mobile robot platform is provided by two symmetric arrangements of linear rails. Each of them has 2 degrees of freedom in the movement plane. On each of them there is a rotating platform actuated by another step-motor. These platforms serve as mounting points for either antennas or targets. With this setup the circular scan was performed with the antennas fixed and the target rotating around its own axis on the rotor platform. This emulated the case where a robot is moving on a circle around a target. The setup of the measurement configuration with its essential devices is sketched in figure 3 for a better overview.

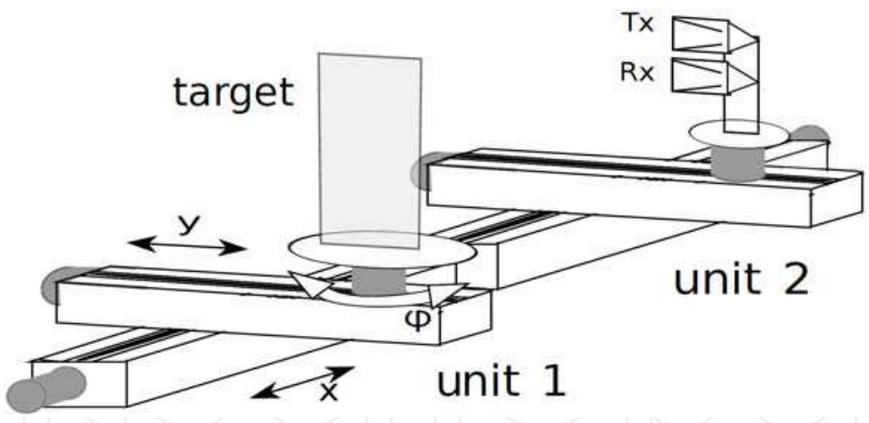

Fig. 3. Layout of the measurement setup with its main devices for experimental validations

Figure 4 shows an example of a simulation-based radargram of object o3 with a triangular cross section. Each object has a specific radar cross section that is strongly angle of radiation dependent. For the purpose of comparison Figure 5 shows the radargram of a real object with same dimensions measured by aforementioned M-Sequence Radar in the passband, i.e 4.5 GHz – 13 GHz. On the left side of both figures 4 and 5 each radargram is determined by a circular track with the object positioned in the centre and the sensors at 1m distance. This is expectedly ideal in the simulated case as both sides of the equal-sided triangular at 45° and 135° cause a specular reflection. However, in the measured radargram of figure 5 a misalignment of the object is noticeable. There is a translative shift of approximately 2 cm to

the centre of rotation which has absolutely no influence onto the whole post-processing at all. As far as the position of the sensors is known, the track can be arbitrarily.

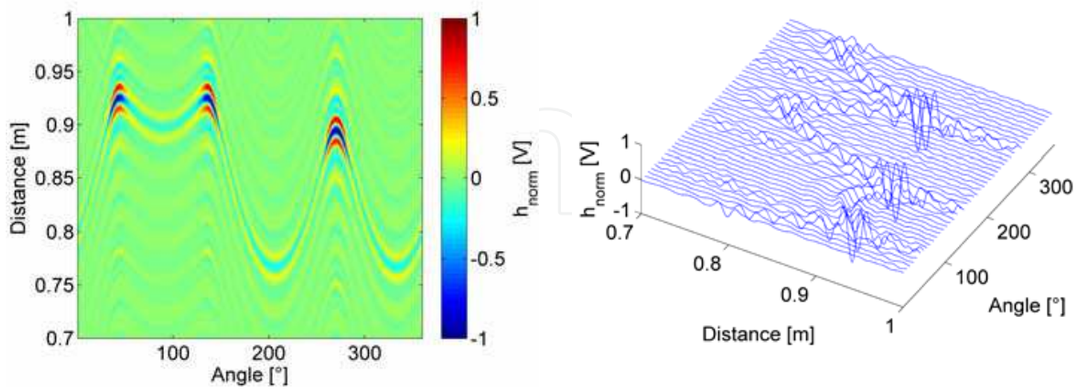

Fig. 4. Radargram of simulated object o3 (left) and every 8th pulse of same Radar data (right)

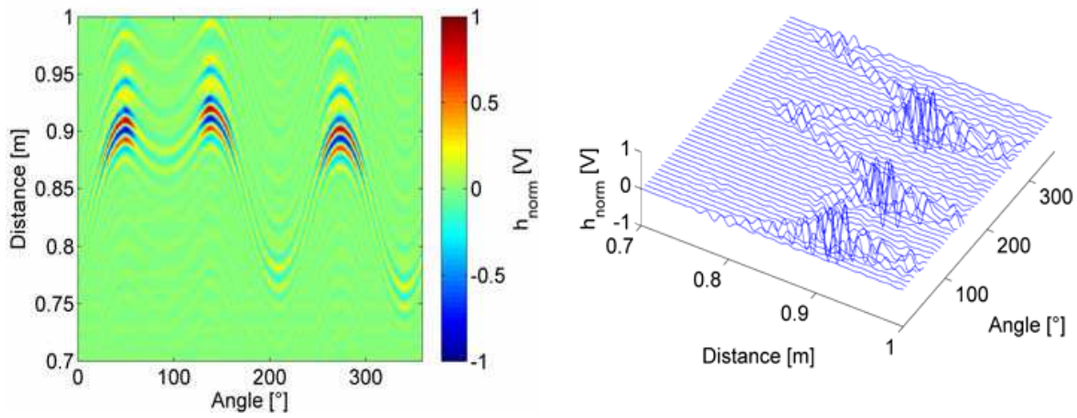

Fig. 5. Measured radargram of object o3 (left) and every 8th pulse of same Radar data (right)

Also for other objects the similarity between simulations and measurements is significantly high. Thus, the performance of the UWB Ray Tracer is verified and serves as basis for further investigations.

2.3 Pre-processing of measured data

Before any algorithm for object reconstruction can be applied, a number of signal processing steps have to be applied onto the raw-data of the M-Sequence Radar device. The raw-data must be up-sampled and up-converted, if the IQ-converter is attached. The signal is provided in the equivalent complex baseband (ECB), as it is usual in high frequency hardware realizations to avoid the effort of high sampling rates. Furthermore, calibration and interpolation is necessary to provide processing-ready data for subsequent algorithms like the imaging and the OR.

In the measured scenario the reference signal is obtained without the object. A reference pulse is needed for the subtraction of the background reflections (clutter) and antenna

crosstalk from the raw signals. The antenna crosstalk is not negligible because the antennas are mounted one above the other at a distance of 12 cm which causes moderate coupling. Moreover, the influence of the microwave devices (e.g. RF switches, RF cables etc.) is compensated by calibration. The interpolation is performed in frequency domain by Fourier transforming the time domain signal. Zero padding and the Hamming window in the frequency domain are applied. After inverse Fourier transforming the time domain signal has finer quantization steps and therewith an improved resolution and a smoother signal form. The Hamming window suppresses sidelobes in the time domain which would appear if a rectangular window was used. Both pre-processing steps are applied and depicted in figure 6.

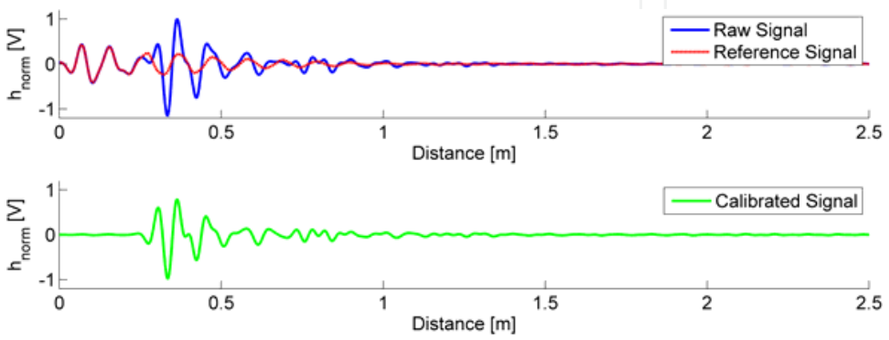

Fig. 6. Interpolated raw signal with antenna crosstalk (above) and calibrated signal after removing the reference signal (below)

Both system signals, i.e. in baseband and passband, are real-valued, as it is usual for every real physically transmitted signal. However, to avoid high sampling rates, as it would be necessary due to Nyquist to sample at least 2 times of the highest appearing frequency, the representation of the passband signal is performed in the ECB. This is essential, because such high frequency digital oscillators are either not available or too expensive. Moreover, it is possible to separate the signal carrier and its information by the complex envelope. The ECB is known to be the down converted version of its analytical Signal in the passband. Let $s_{PB}(t)$ be a real valued passband signal, e.g. the Radar signal with attached up/down converter, then

$$s^{+}_{PB}(t) = s_{PB}(t) + j \cdot \hat{s}_{PB}(t) \tag{1}$$

is the analytical signal, with

$$\hat{s}(t) = H\{s(t)\} = f^{-1}\{-j \cdot \mathrm{sgn}(\omega) f\{s(t)\}(\omega)\}(t) \tag{2}$$

being the Hilbert transform of s(t) expressed by the Fourier transform. Here $f\{\bullet\}$ is the Fourier transform and $H\{\bullet\}$ the Hilbert transform. Obviously, an analytical signal is a signal whose imaginary part is the Hilbert transform of its real part. The ECB signal $s_{ECB}(t)$ can be expressed as

$$s_{ECB}(t) = s^{+}_{PB}(t) e^{-j2\pi f_0 t}. \tag{3}$$

Here, f_0 is the carrier frequency. In the spectrum it leads to

$$S_{\mathrm{ECB}}(\omega) = S^{+}_{\mathrm{PB}}(\omega + \omega_0). \tag{4}$$

3. Highly accurate wavefront detection

To achieve super-resolution of the Radar system, wavefronts have to be detected accurately and, in case of multiple reflections, overlapping pulses must be separated by a suitable algorithm. A wavefront is a curve within the radargram where each point on the curve indicates the distance at which a reflective feature of the object, visible from the sensor setup, is located. A reflective feature can either be a smooth, large (in comparison to the smallest wavelength) plane or edges and corners, which cause scattering and retroreflection, respectively. Based on the speed of light value these wavefronts are used to determine the distance between the reflecting point and the sensor. In this work, these distances are used in subsequent algorithms to extract a Radar image and to enable the OR. The highly accurate wavefront detection becomes a challenging task when it deals with multi-scattering conditions. This is the case when complicated objects have surface variations less than a wavelength or have many concave and convex edges like the objects o5 – o12. Distortion is caused by richly interfered signals scattered from multiple scattering centres of the object surface. This results in constructive and destructive interference which leads to deformation of the pulse. In this section two algorithms shall be introduced in detail which have proven to be robust and efficient, i.e. a correlation based method and an optimization problem solved by a genetic algorithm.

In both algorithms, again a reference pulse is needed. The double-ridged horn antennas used in this work have 20° opening angle to the left and right, respectively. The amplitude of the transfer function within this area, and therewith the attenuation, is marginal and negligible. Since the cross-range resolution is proportional to the wavelength and inverse proportional to the aperture, measurements in the passband are chosen to provide lower wavelengths and therewith finer resolution. A set of reference pulses is shown in figure 7 which were obtained as reflection against a cylinder (diameter 9 cm) and a large metal plate, respectively. For the purpose of comparison, they are normalised in amplitude and delay.

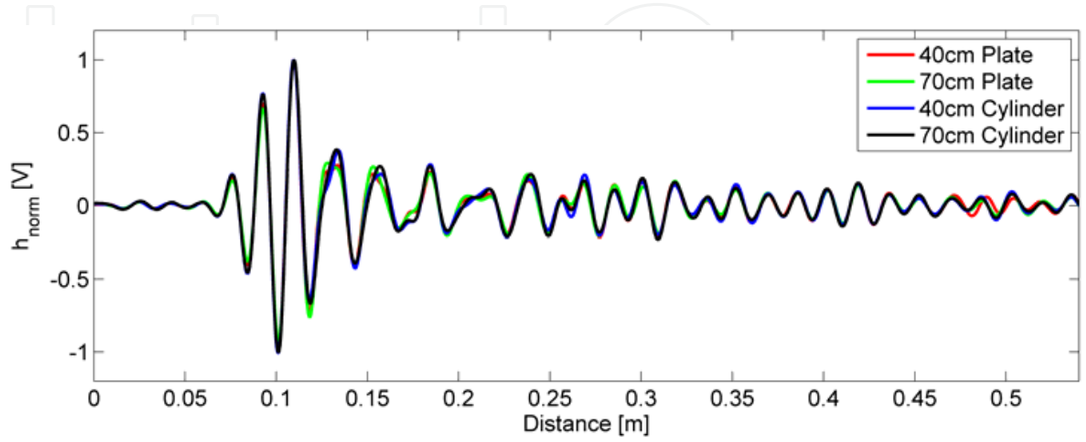

Fig. 7. A set of reference pulses taken at different distances against a plate and cylinder with normalised amplitude and delay

Once a wavefront has been detected in a signal under test, the distance has to be extracted accurately. A distinctive part of the reference pulse has to be marked as the location or moment respectively, when the reflection takes place at the objects surface. Assume $ref(t)$ to be the reference pulse then usually $\max\{|ref(t)|\}$ is set to be the point, or moment respectively, in which the reflection actually takes place. This point has the maximum instantaneous energy detected by the sensor which corresponds with the reflection. However, an adaption to the Radar data can be necessary with a change of the sign of the reference pulse. This depends on the sign of the maximum amplitude of the radar data which was within these investigations negative. For further processing it makes sense to shift the reference pulse such that $\max\{|ref(t)|\}$ is in the origin of the time-axis. This leads to the reference pulse used in this work and is shown in figure 8.

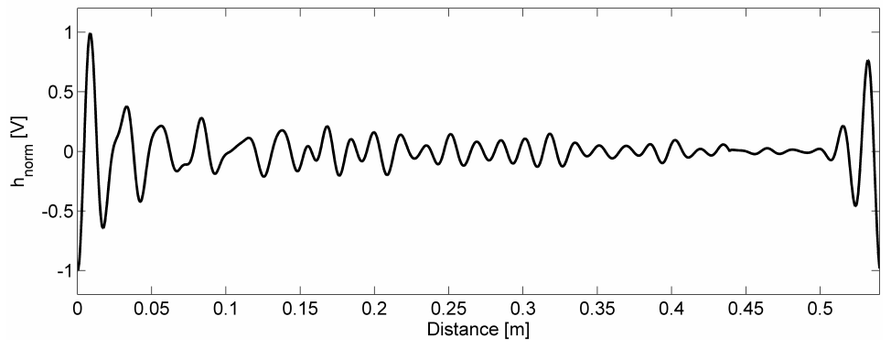

Fig. 8. calibrated and normalised reference pulse used in this work

3.1 Correlation based wavefront detection – the matched filter principle

The basic idea of this algorithm, first introduced in (Hantscher et al., 2007) is to locate echoes iteratively by evaluating the normalized cross-correlation function of the signal under test with an offline determined reference pulse. The maximum of this cross-correlation function indicates the shift with which the reference pulse has highest similarity within the signal under test. Once a wavefront is extracted, the algorithm recursively subtracts scattered pulses to resolve multiple echoes. This step is iterated on the resulting signal until a termination condition is fulfilled. The termination condition is determined heuristically, e.g. when a certain difference in the signal power before and after subtraction is reached, or simply when a fixed number of wavefronts are of interest or, as it was the case within this work, when the normalized correlation coefficient which equals 0 for orthogonal signals and 1 for identical ones, is less a threshold, e.g. 0.5 . The correlation coefficient for the 1st wavefront (i=1) is

$$ccf_{\text{echo,i}}(t_d) = \frac{\sum_{k=1}^{K} s_i(t_k) \cdot ref(t_k - t_d)}{\sqrt{\sum_{k=1}^{K} \left(s_i(t_k)\right)^2} \cdot \sqrt{\sum_{k=1}^{K} \left(ref(t_k)\right)^2}} \tag{7}$$

with time samples t_k, the mean-value free reference signal $ref(t_k)$ and mean-value free signal under test $s_i(t_k)$. $ccf_{\text{echo},1}(t_d)$ is proportional to the cross correlation function and

represents the correlation coefficient for each time delay t_d normalized by the RMS values of $s_i(t_k)$ and $ref(t_k)$. The normalization avoids the problem of higher signal energies resulting in higher correlation values. The parameter

$$\Delta t_{echo,i} = \arg\max_{t_d}\left(\left|ccf_{echo,i}(t_d)\right|\right) \tag{8}$$

contains the time difference between the first detected reflection and the calibrated reference pulse, i.e. the moment at which the reference signal matches best the signal under test. Actually, because of the calibration of the reference pulse in figure 8 $\Delta t_{echo,i}$ equals the round trip time, or in combination with the velocity of light, the distance from the sensors to the reflecting centre. In order to investigate the signal under test for further reflections, the earlier detected wavefront has to be removed coherently since it covers other reflections. A scaling factor

$$s_f = \frac{s(\Delta t_{echo,i})}{ref(t_k - \Delta t_{echo,i})} \tag{9}$$

is estimated by taking the ratio of the amplitudes of the detected wavefront and the reference pulse at the point of maximum correlation. This scaling factor gives an estimation with which amplitude the reference signal has to be removed from the signal under test. This substraction operation provides the new signal under test

$$s_{i+1}(t_k) = s_i(t_k) - s_f \cdot ref(t_k - \Delta t_{echo,i}), \tag{10}$$

which then will be analysed for further wavefronts. Similarly, further wavefronts are extracted iteratively by repeating equation (7) and the adjacent ones. This strategy can be considered as the matched filter principle with the reference pulse as the impulse response of the pulse shaping filter of the transmitter as well as the one of the receiver. This parameter estimation scheme maximizes the signal-to-noise power ratio.

3.2 Wavefront detection by a genetic algorithm

The correlation based wavefront detection works excellent for single simple shaped objects (e.g. o1-o4) or several simple objects which are separated by distances of several wavelengths. The small computation effort satisfies real time conditions and the range resolution is in sub centimetre range. Under these assumptions interference is negligible and waveforms are not distorted very much. However, for complex shaped objects which cause multiple reflections, wavefronts can interfere with each other. Especially when the overlap range is within a pulsewidth, constructive and/or destructive interference are hardly separable.

For scenarios with multiple scattering conditions a genetic optimization algorithm (GA) for modelling the impulse response has proven to be very efficient. Hence, the pulse separation task is formulated as a multidimensional optimization problem and extracts even interfering pulses. Because of multimodality and complexity analytical approaches are not appropriate in every case. Here, GA has been proven to be a powerful tool by applying a heuristic search (Johnson & Rahmat-Sammi, 1997). The GA used in this paper is similar to (Hantscher & Diskus, 2009). The main difference is that the sensors in this work have no angle

dependence, because they have narrow main lobes resulting in an aperture with negligible incident angle.

The basic idea of the GA is that the signal under test $s(t_k)$ with time samples t_k and index k is assumed to be described by a superposition of shifted and weighted reference pulses $ref(t_k)$. The set of reference pulses which vary by different parameters weight w_g and delay d_g of the g[th] wavefront, shall approximate $s(t_k)$ best with every meaningful combination of both parameters. A meaningful quality criterion can e.g. be the least square value. In contrast to the correlation based algorithm, the number of wavefronts G has to be presumed and was set to 3 within these investigations. The block diagram of the GA process is shown in figure 9.

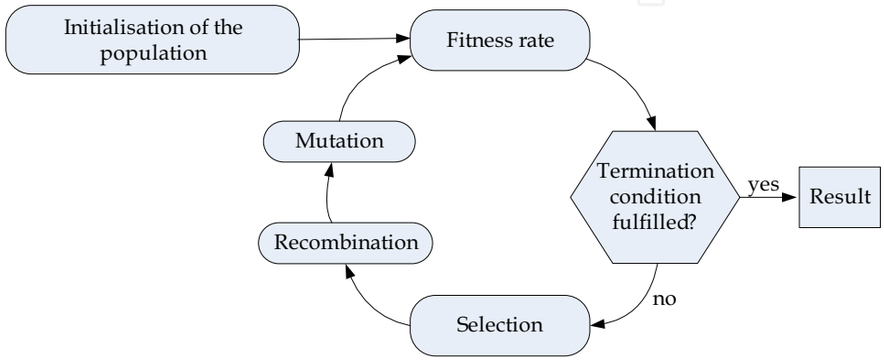

Fig. 9. Block diagram of the used GA for wavefront detection

Firstly, the GA starts for every signal under test with an initialisation of a population of N individuals. Each individual resembles a potential solution of the optimisation problem. Here, every individual comprise the parameters weight w_g and delay d_g to provide a potential solution

$$c(t_k) = \sum_{g=1}^{G} w_g \cdot ref(t_k - d_g). \tag{11}$$

The parameters w_g and d_g are assigned uniformly distributed in the initialisation of the population. For example d_g should be close to the area where the object is supposed to be and w_g should be in relation to used power levels. The number of individuals is chosen to be N = 200. Figure 10 shows an assembly of such a population for a better overview.

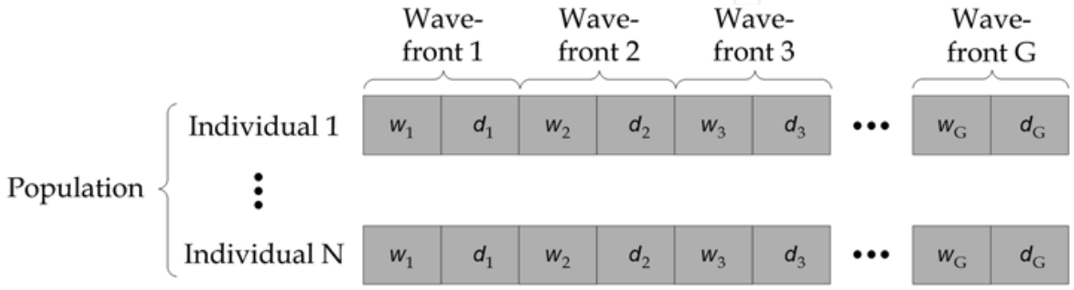

Fig. 10. A population of N individuals with G wavefronts

In the next step the quality of the approximation is determined by means of a fitness function, i.e. the difference between of the signal under test and each individual in the least square sense

$$F = \sqrt{\frac{1}{\mathrm{K}}\sum_{\mathrm{k}=1}^{\mathrm{K}}\left(s(\mathrm{t_k}) - c(\mathrm{t_k})\right)^2} = \sqrt{\frac{1}{\mathrm{K}}\sum_{\mathrm{k}=1}^{\mathrm{K}}\left[\left(s(\mathrm{t_k}) - \sum_{\mathrm{i}} w_{\mathrm{i}} \cdot ref\left(\mathrm{t_k} - d_i\right)\right)\right]^2} \cdot \tag{12}$$

$\rightarrow \min \qquad\qquad \rightarrow \min$

After having calculated the fitness of each individual, it is decided whether the termination condition of the GA is fulfilled. In (Hantscher & Diskus, 2009) the difference between the fitness of the best and the fitness of the worst is less than a threshold, of e.g. 2%. However, numerous simulations and measurements show that this strategy can break the GA off too early or hung up in an infinite loop. To take a constant number of iterations has proven more efficient. If the termination condition is not fulfilled the next step "selection" is applied. Before the recombination can be carried out, the required individuals have to be chosen here. The worst N/2 individuals are removed from the population and the remaining N/2 individuals are selected for the recombination. The remaining individuals form randomly N/4 sets of parents and each produce 2 children by a so called one-point crossover. This results again in a population of N individuals. The one-point crossover works as follows. Every set of parents is split after a random set of parameter into two parts. Then, all parameter beyond that cut are swapped within both parents resulting in two new individuals called children. This procedure is repeated with every set of parents. Figure 11 shows the principle of the one-point crossover.

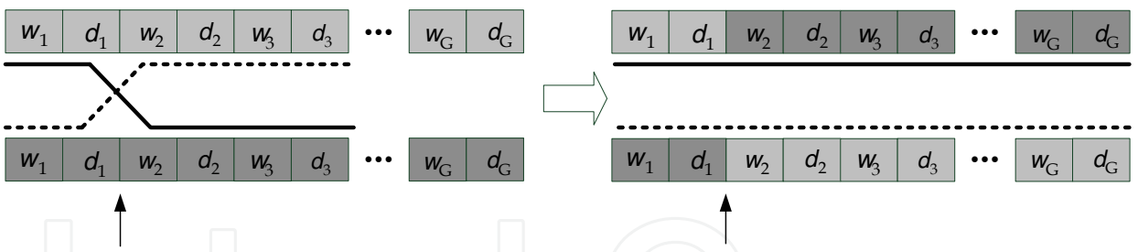

Fig. 11. Operation of the one-point crossover method

Finally, the mutation operation is applied onto the new population. The algorithm is guarded against getting stuck in a local minimum by changing the parameters w_{g} and d_{g} slightly. To the delay d_{g} a normally distributed random number with a mean of 0 is added and the weight w_{g} is multiplied with a normally distributed random number with a mean of 1. Both standard deviations should be chosen adaptively. At the beginning of iterations a high standard deviation secures the genetic deviation, whereas a low standard deviation at the end causes a fine tuning of the solutions. Finally, the GA calculates again the fitness of each individual and starts another iteration until the determination condition is fulfilled (maximum number of iterations). The result is the individual with lowest mean square error with which the signal under test can be reconstructed in an approximated type.

The number of wavefronts G was set to 3 within these investigations which satisfied resolution assumptions. Even for signals with only one wavefront, the remaining two wavefronts were located around the actual one because of the fitness conditions. Hence, a simple filter which connects two nearby wavefronts was sufficient to complete the GA results.

In the following a couple of results for both wavefront detection algorithms are shown. Figure 12 deals with object o5. The radargrams and additionally the detected wavefronts are depicted. The threshold for the correlation coefficient was set to 0.4 .

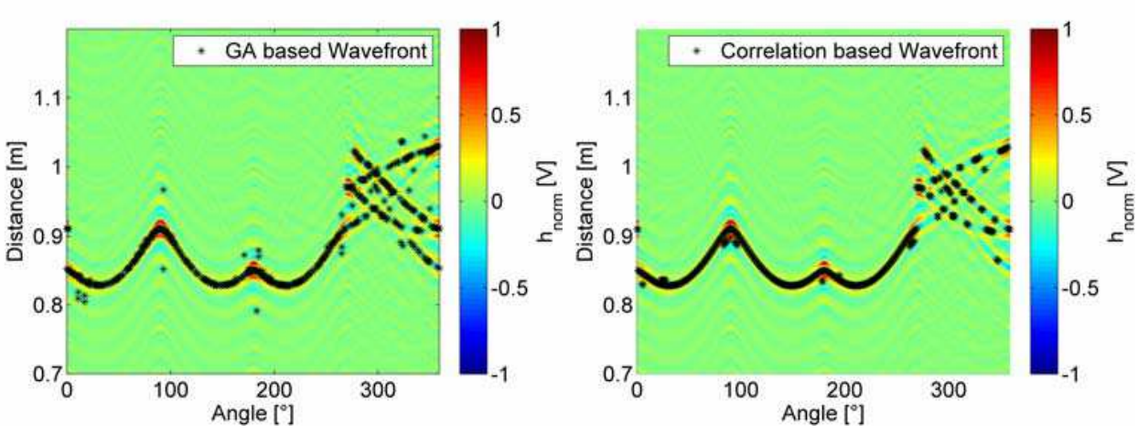

Fig. 12. Detected wavefronts by both algorithms for object o5

To demonstrate the quality of estimating the wavefront the 289th impulse response of figure 12 was reconstructed by superpositioning the weighted and shifted wavefronts of both algorithms.

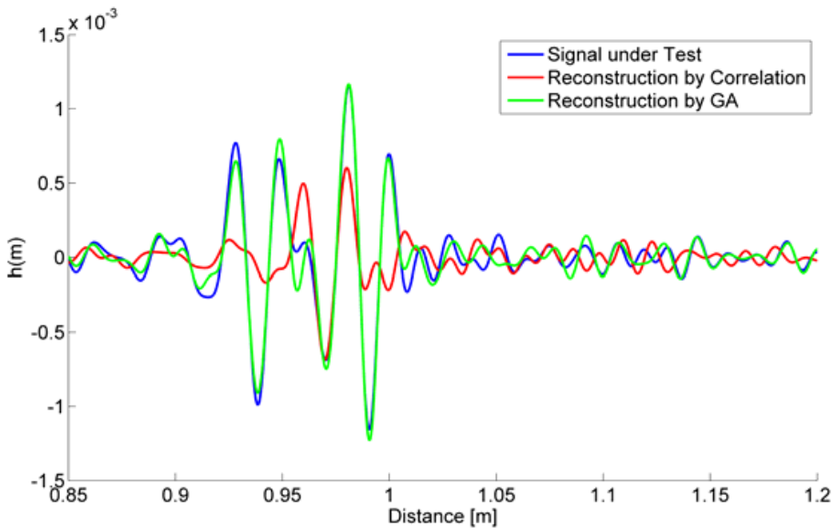

Fig. 13. Reconstruction of a signal under test with both wavefront detection algorithms

Obviously, and this is what was proven with numerous simulations and measurements with numerous objects, the GA performs more efficient under multi scattering conditions

than the correlation algorithm. However, if the object is most probably a simple one without edges, corners and high variations, then the correlation algorithm should be preferred because of time saving. But normally, a Radar image is performed for unknown objects and in this cases the GA provides more precise wavefront detections.

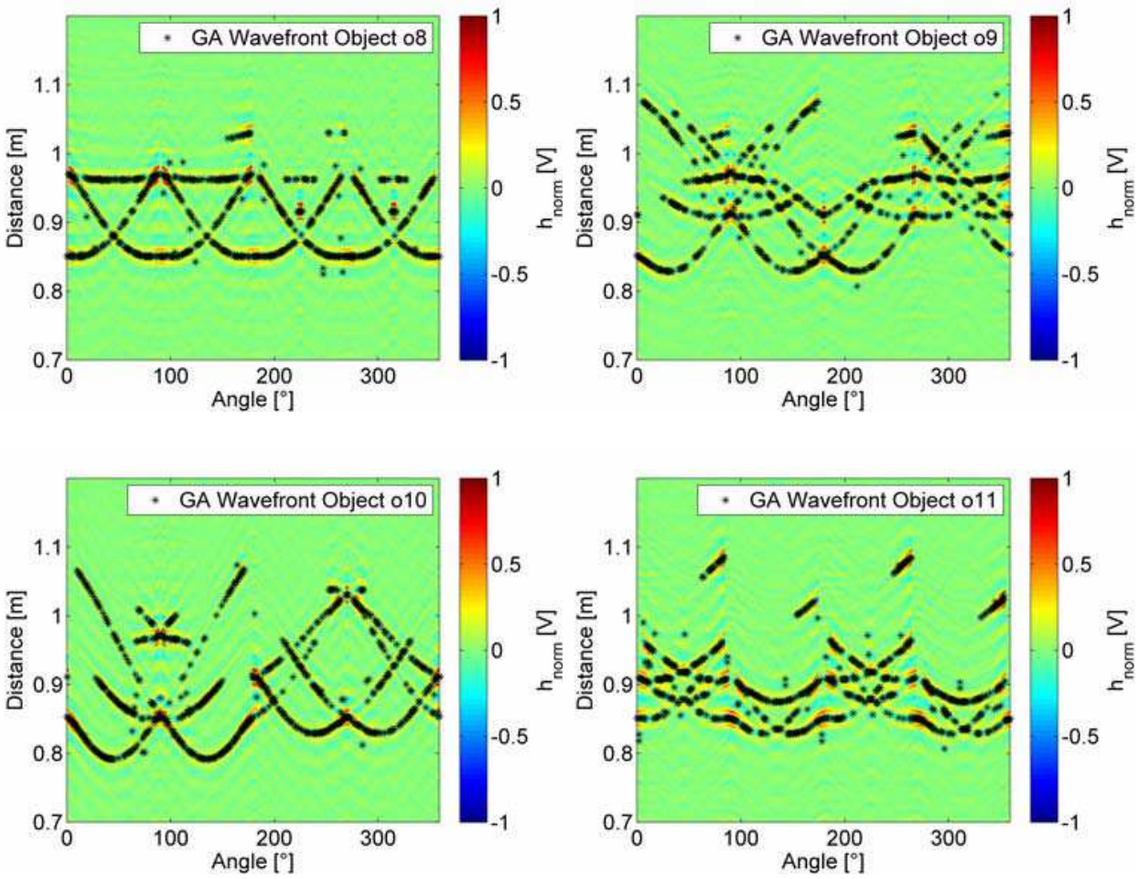

Fig. 14. Examples of some radargrams including detected wavefronts with the GA

4. Super resolution UWB imaging

A large variety of imaging algorithms was designed, mostly based on migration techniques (Hantscher et al., 2006; Zetik et al., 2005), Synthetic Aperture techniques (McIntosh et al., 2002) which are related close to the migrations, time-reversal algorithms (Liu et al., 2007) and other optimization algorithms (Massa et al., 2005). However, these algorithms are inappropriate for emergency scenarios because of the immense computational load excluding real-time conditions. Even though, these obtained images have inadequate image resolution and need further processing to extract an object contour. In contrary, it was shown that the inverse boundary scattering transform (IBST) which is given by

$$\begin{cases} x(x_w) = x_w - z_w \cdot dz_w / dx_w \\ z(x_w) = z_w \cdot \sqrt{1 - (dz_w / dx_w)^2} \end{cases} \tag{13}$$

and IBST inspired algorithms are a simpler and more computationally efficient UWB imaging algorithm which determines the direction of Radar responses based on changes of the round-trip times (RTT) and thus performs a direct imaging. Here, x and z are the coordinates of the final radar image which contains the shape of the object. The variable z_w represents the distance of the wavefront to the antenna position x_w. Therefore, the IBST requires only the knowledge of the round-trip times of the wavefronts at every antenna position. Since the introduction of the original IBST in 2004 (Sakamoto & Sato, 2004) there has been significant research effort for improvements by extending it to 3-D, bistatic configurations and non-planar tracks (Helbig et al., 2008) for imaging the outer surface of a target and even for medium penetrating in-wall imaging (Janson et al., 2009).
However, IBST utilizes the derivative of the received data and hence is sensitive to noise. Moreover it is hard to apply for complex objects with multi-scattering behaviour and discontinuous wavefronts, as it is the case for objects o5 – o12.
In (Kidera et al., 2008) an imaging algorithm was proposed that utilizes fuzzy estimation for the direction of arrival (DOA). It extracts a direct mapping by combining the measured distance of the wavefront with its DOA. Moreover it realizes a stable imaging of even complex objects and requires neither preprocessing like clustering or connecting discontinuous wavefronts, nor any derivatives. The angular estimation of the DOA relies on the convergence of nearby wavefronts to the wavefront under test if the antenna positions of those nearby wavefronts move towards the regarding one. A membership function

$$f(\theta, X_\mathrm{i}, Z_\mathrm{i}) = \mathrm{e}^{-\frac{\left\{\theta - \theta(X_\mathrm{i}, Z_\mathrm{i})\right\}^2}{2\sigma_\theta^2}}, \tag{14}$$

is utilized where $\theta(X_\mathrm{i}, Z_\mathrm{i})$ is defined as the angle between the intersection point of the regarded wavefront circle with the neighbouring wavefront of the i$^{\mathrm{th}}$ antenna position and the x-axis. This is performed for all possible $\theta = 0° \ldots 359°$ and for $\mathrm{i} = 1 \ldots N$ with N neighbouring wavefronts which intersect the wavefront circle of the regarded one. The angular estimation of the wavefront under test is calculated by

$$\theta_{\mathrm{opt}} = \arg\max_{\theta} \left\{ s(X_\mathrm{i}, Z_\mathrm{i}) f(\theta, X_\mathrm{i}, Z_\mathrm{i}) \mathrm{e}^{-\frac{\left\{X - X_\mathrm{i}\right\}^2}{2\sigma_\mathrm{x}^2}} \right\}, \tag{15}$$

where $s(X_\mathrm{i}, Z_\mathrm{i})$ is the signal amplitude of the i$^{\mathrm{th}}$ antenna position and σ_x and σ_θ are empirically determined constants. The crucial parameters of this algorithm are σ_x and σ_θ which can be considered to be the standard deviation of the exponential terms having Gaussian curvature. Hence, σ_x and σ_θ determine the width of this Gaussian curvature and therewith its focus. However, depending on the chosen value of σ_x and σ_θ more or less influence of wavefronts of neighbouring antenna positions can be taken into account which results either in images of rather smooth and straight planes or, in contrast, highlight edges and corners. Figure 15 shows the case in which the edges are highlighted by the algorithm.

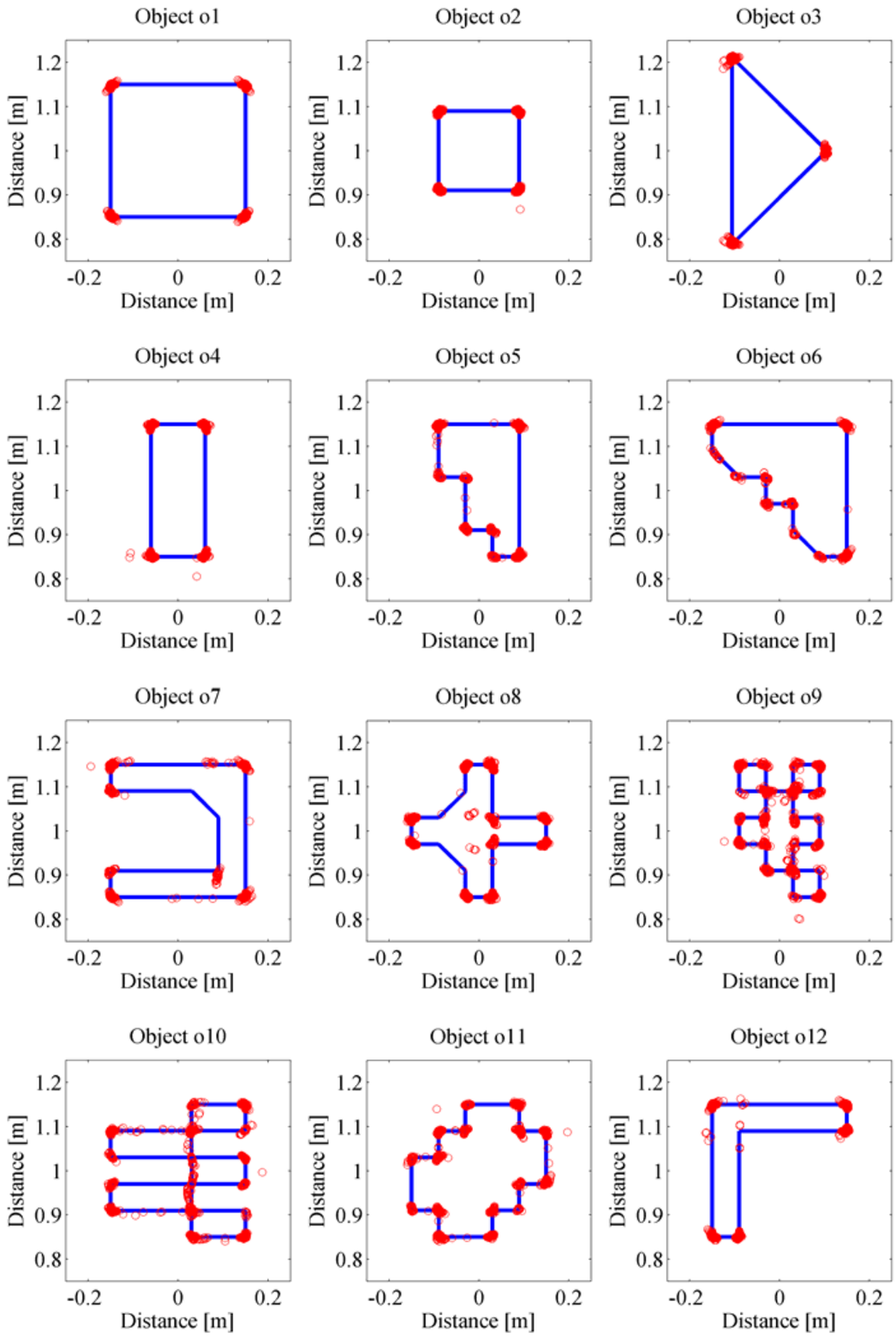

Fig. 15. Raw images determined by the imaging algorithm and the object contour

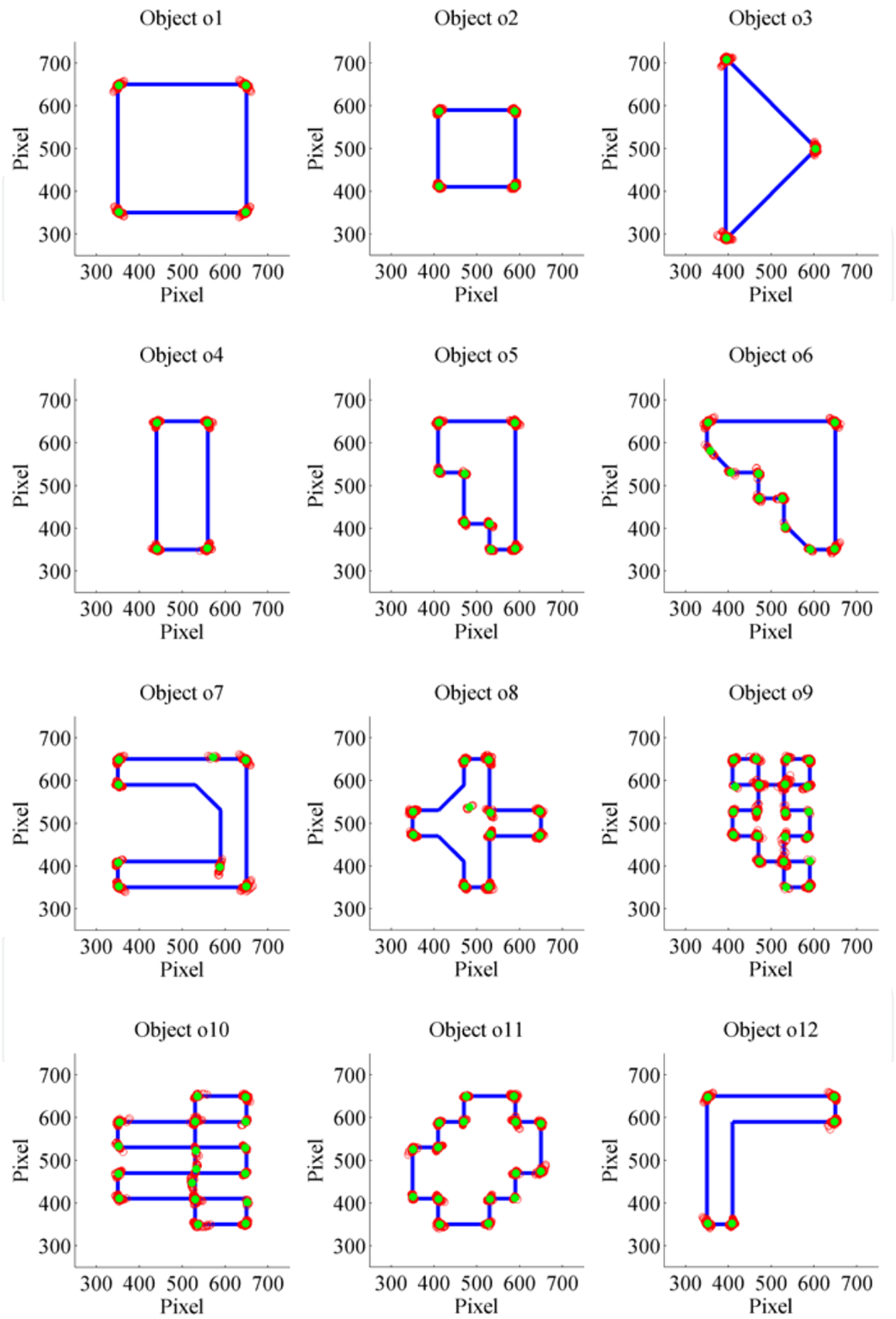

Fig. 16. Clustered and filtered images ready for the OR processing

4.1 Post processing of raw images

In order to perform the OR the UWB image has to be adapted to the reference alphabet of chapter 2.1. Hence, the values of the imaging parameters σ_x and σ_θ are chosen with a low value and a post processing in terms of filtering and clustering is applied. At first, a clustering is performed to merge image pixels of one edge or corner to one cluster. In case the image consists of *K* image pixels with Cartesian coordinate $P_j(x,y)$ for the j-th pixels, then every pixel for which

$$\left|P_m - P_n\right| \leq 1\,\mathrm{cm} \qquad \forall\, m=n=[1;K] \tag{16}$$

holds, are merged to one cluster. A filtering is performed by deleting clusters with less then 4 pixels to avoid isolated image pixels. For every remaining cluster the centre of mass is calculated which is the representative of the corresponding edge or corner. Thus, the pixel at the centre of mass of every cluster is set a value of 1. The remaining pixels are set to 0. Both post processing steps are applied onto the raw images, the results are shown in figure 16.

5. Object recognition algorithm

5.1 Moment based feature

The image moments are calculated by the invariant moment algorithm (Chen, 1993). Based on 5 central moments $\mu_{p,q}$ 7 other moments φ_i can be determined which are invariant to translation, rotation and scaling. Here, shape parameters of the object are extracted based on the objects geometry and its distribution of pixels. The invariant moments are determined for every object both of the reference alphabet and the post processed images.

5.2 Texture based feature

The texture feature consists of polar Fourier descriptors (FD). The parameterization of the boundary line is not any more expressed by a path length *p*, instead the angle Φ between the radius from the center of mass to a point on the boundary and the x-axis is used. However, the straight segments between corners and edges have to be sampled equiangular for the recognition process with polar Fourier descriptors. Therefore the pixel with the value of 1 of each reference image are connected in ascending angular order. These connections are afterwards sampled equiangular resulting in a series of 360 values which equal 360 radii. The resulting polar signature with a one degree grid is used and a Fourier Transformation is applied onto the resulting $N = 360$ real valued series. The obtained coefficients are known as the polar FD of the object boundary. The resulting *N* wave number coefficients run from 0 to N-1, or respectively due to Nyquist from $-N/2$ to $N/2$-1. In contrast to classical FD the polar FD are translation and rotation invariant if the absolute values of the coefficients are regarded. However, the 0-th coefficients of the polar FD represent the mean radius. Hence, the polar FD can be made scale invariant by normalizing all coefficients with reference to the 0-th one. In this work this is not done, because o1 and o2 both are squares just with different dimension and shall be treated as 2 different objects.

5.3 Geometrical features

Geometrical features are obtained both for the reference alphabet and the images of the object under test. The translation and rotation invariant geometrical features are:

- Total mass of the image
- Eccentricity
- Bounding circle
- Form factor

The total mass is the sum of the pixels belonging to the object. In case of binary images it is the sum of all pixel-values in the image. The eccentricity is based on 2nd order moments and ranges from 0 to 1. It is a measure for the circularity of an object. The bounding circle is defined as the circumference of the circle which is just large enough to contain all object pixels. The form factor is the relation between the bounding circle and the total mass of the image and is a measure for the compactness of the image.

5.4 Combined object recognition

Each image under test is compared against every 12 reference images by a MSE classifier applied to all six features. Hence, every object under test has six 1 by 12 error-vectors $\vec{e}_{\mathrm{i}} \quad \forall\, \mathrm{i}=1\ldots6$ with MSE values for each of the 12 compared combinations and for all 6 features. For reasons of expressing a recognition rate in probabilities all $\vec{e}_{\mathrm{i}}$ of every object are mapped to a probability vector

$$\vec{p}_{\mathrm{i}}(j) = \mathrm{e}^{-\frac{\vec{e}_{\mathrm{i}}(j)^2}{0.1\mathrm{std}(\vec{e}_{\mathrm{i}})^2}} \qquad \forall j = 1\ldots12 \ \wedge\ \mathrm{i} = 1\ldots6 \tag{17}$$

with std(.) as the standard deviation. To achieve a cumulative probability of 1 per object and per feature, each $\vec{p}_{\mathrm{i}}$ is normalized to

$$\vec{p}_{\mathrm{norm,i}}(j) = \frac{\vec{p}_{\mathrm{i}}(j)}{\sum_{m=1}^{12} \vec{p}_{\mathrm{i}}(m)} \qquad \forall j = 1\ldots12 \ \wedge\ \mathrm{i} = 1\ldots6. \tag{18}$$

Then, after multiplicative combination of every feature with

$$\arg\max_{j} \left\{ \prod_{\mathrm{i}=1}^{6} \vec{p}_{\mathrm{norm,i}}(j) \right\} \qquad \forall j = 1\ldots12, \tag{19}$$

a joint OR probability can perform a recognition of the jth reference object for the object under test.

6. Results and conclusion

In this chapter a robust UWB OR algorithm is presented which is based on super-resolution UWB imaging. Geometrical features are extracted and used in a joint maximum probability algorithm. After combining geometrical features with the moment invariant algorithm and the Fourier descriptors, both OR algorithms can recognize all 12 objects correctly. In every case the probability for the 1st failure (or the 2nd probable object) was significantly smaller than the correct decision.

7. Acknowledgement

The authors thank the Deutsche Forschungsgemeinschaft (DFG) for the support of the work as part of the "Cooperative Localisation and Object Recognition in Autonomous UWB Sensor Networks" (CoLOR) project within the UKoLoS priority program.

8. References

Chen, C. C. (1993). Improved moment invariants for shape discrimination, *Pattern Recognition Journal,* Vol. 26, No. 5, 1993, pp. 683-686.

Geng, N. & Wiesbeck, W. (1998). *Planungsmethoden für die Mobilkommunikation,* Springer Verlag, ISBN 3540647783, Berlin, 1998.

Hantscher, S.; Reisenzahn, R. & Diskus, C. (2006). Analysis of Imaging Radar Algorithms for the Identification of Targets by Their Surface Shape, *IEEE International Conference on Ultra-Wideband, ICUWB 2006*, Waltham, USA, Oct. 2006.

Hantscher, S.; Etzlinger, B.; Reisenzahn, A. & Diskus, C. G. (2007). A Wavefront Extraction Algorithm for High-Resolution Pulse Based Radar Systems, *IEEE International Conference on Ultra-Wideband, ICUWB 2007*, Singapore, Sep. 2007.

Hantscher, S & Diskus, C. G. (2009). Pulse-Based Radar Imaging Using a Genetic Optimization Approach for Echo Separation. *IEEE Sensors Journal.*Vol. 9, No. 3, March 2009, pp. 271–276.

Helbig, M.; Hein, M.A.; Schwarz, U. & Sachs, J. (2008). Preliminary investigations of chest surface identification algorithms for breast cancer detection", *IEEE International Conference on Ultra-Wideband, ICUWB 2008*, Hannover, Germany, Sept. 2008.

Janson, M.; Salman, R.; Schultze, Th.; Willms, I.; Zwick, T. & Wiesbeck, W. 2009. Hybrid ray racing/FDTD UWB model for object recognition. *Frequenz Journal of RF-Engineering and Telecommunications*, Vol. 63, No. 9/10, Sept./Oct. 2009, pp. 217-220.

Johnson, J. M. & Rahmat-Sammi, Y. (1997). Genetic Algorithm in Engineering Electromagnetics. *IEEE Antennas and Propagation Magazine*. Vol. 39, No. 4, Aug. 1997, pp. 7 – 25.

Kidera, S.; Sakamoto, T. & Sato, T. (2008). High-Speed UWB Radar Imaging Algorithm for Complex Target Boundary without Wavefront Connections. *XXIX General Assembly of the International Union of Radio Science (URSI)*, Chicago, Illinois, USA, Aug. 2008.

Liu, D.; Krolik, J. & Carin, L. (2007). Electromagnetic target detection in uncertain media: Time-reversal and minimum-variance algorithms. *IEEE Transactions on Geoscience and Remote Sensing.* Vol. 45, No. 4, April 2007, pp. 934-944.

Massa, A.; Franceschini, D.; Franceschini, G.; Pastorino, M.; Raffetto, M. & Donelli, M. (2005). Parallel GA-based approach for microwave imaging applications. *IEEE Transactions on Antennas and Propagation.* Vol. 53, No. 10, Oct. 2008, pp. 3118-3127.

McIntosh, J.S.; Hutchins, D.A.; Billson, D.R.; Noble, R.A.; Davies, R.R.; Koker, L. (2002). SAFT Imaging Using Immersed Capacitive Micromachined Ultrasonic Transducers, *International Ultrasonics Symposium*, Munich, Germany, Oct. 2002.

Sachs, J.; Kmec, M.; Zetik, R.; Peyerl, P.; Rauschenbach, P. (2005). Ultra Wideband Radar Assembly Kit. *IEEE international Geoscience and Remote sensing Symposium, IGARS 2005,* Seoul, Korea, July 2005.

Sakamoto, T. & Sato T. (2004). A target shape estimation algorithm for pulse radar systems based on boundary scattering transform. *IEICE Transactions on Communications*. Vol. E87-B, No.5, May 2004 , pp.1357-1365.

Salman, R.; Schultze, Th. & Willms, I. (2010). Performance Enhancement of UWB Material Characterisation and Object Recognition for Security Robots. *Journal of Electrical and Computer Engineering*. Vol. 2010, Article ID 314695, 6 pages, 2010.

Schultze, Th.; Porebska, M.; Wiesbeck, W. & Willms, I. (2008). Onsets for the Recognition of Objects and Image Refinement using UWB Radar, *German Microwave Conference, GEMIC 2008*, Hamburg-Harburg, Germany, March 2008.

Zetik, R.; Sachs, J. & Thomä, R. (2005). Imaging of Propagation Environment by Channel Sounding, *XXVIIIth General Assembly of URSI*, New Delhi, India, Oct. 2005.

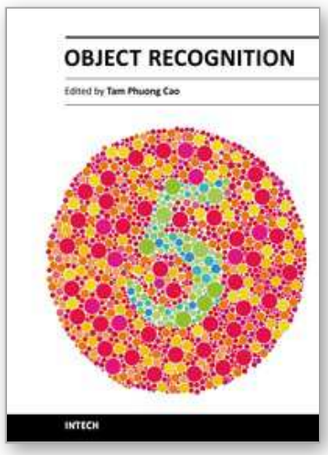

Object Recognition

Edited by Dr. Tam Phuong Cao

ISBN 978-953-307-222-7
Hard cover, 350 pages
Publisher InTech
Published online 01, April, 2011
Published in print edition April, 2011

Vision-based object recognition tasks are very familiar in our everyday activities, such as driving our car in the correct lane. We do these tasks effortlessly in real-time. In the last decades, with the advancement of computer technology, researchers and application developers are trying to mimic the humanâ€™s capability of visually recognising. Such capability will allow machine to free human from boring or dangerous jobs.

How to reference

In order to correctly reference this scholarly work, feel free to copy and paste the following:

Rahmi Salman and Ingolf Willms (2011). Super-Resolution Object Recognition Approach for Complex Edged Objects by UWB Radar, Object Recognition, Dr. Tam Phuong Cao (Ed.), ISBN: 978-953-307-222-7, InTech, Available from: http://www.intechopen.com/books/object-recognition/super-resolution-object-recognition-approach-for-complex-edged-objects-by-uwb-radar

INTECH
open science | open minds

InTech Europe
University Campus STeP Ri
Slavka Krautzeka 83/A
51000 Rijeka, Croatia
Phone: +385 (51) 770 447
Fax: +385 (51) 686 166
www.intechopen.com

InTech China
Unit 405, Office Block, Hotel Equatorial Shanghai
No.65, Yan An Road (West), Shanghai, 200040, China
中国上海市延安西路65号上海国际贵都大饭店办公楼405单元
Phone: +86-21-62489820
Fax: +86-21-62489821

IntechOpen